European Polymer Journal 121 (2019) 109294

Contents lists available at ScienceDirect

European Polymer Journal

journal homepage: www.elsevier.com/locate/europolj

The influence of elastomeric polyurethane type and ratio on the physicochemical properties of electrospun polyurethane/silk fibroin hybrid nanofibers as potential scaffolds for soft and hard tissue engineering

Najmeh Dehghan-Manshadi[a], Saeid Fattahi[a], Mohsen Hadizadeh[a], Habib Nikukar[b,c,*], Seyed Mohammad Moshtaghioun[d,e], Behrouz Aflatoonian[b,c,e,f]

[a] Textile Engineering Department, Faculty of Engineering, Yazd University, Yazd, Iran
[b] Medical Nanotechnology and Tissue Engineering Research Center, Yazd Reproductive Sciences Institute, Shahid Sadoughi University of Medical Sciences, Yazd, Iran
[c] Department of Advanced Medical Sciences and Technologies, School of Paramedicine, Shahid Sadoughi University of Medical Sciences, Yazd, Iran
[d] Biology Department, Faculty of Science, Yazd University, Yazd, Iran
[e] Stem Cell Biology Research Center, Yazd Reproductive Sciences Institute, Shahid Sadoughi University of Medical Sciences, Yazd, Iran
[f] Department of Reproductive Biology, School of Medicine, Shahid Sadoughi University of Medical Sciences, Yazd, Iran

ARTICLE INFO

Keywords:
Elastomeric polyurethane
Silk fibroin
Hybrid nanofibers
Electrospinning
Physicochemical properties
Soft and hard tissue engineering

ABSTRACT

Hybrid materials and structures have been known as multifunctional polymers used for various commercial productions. Recently, biomaterials have become an emerging research field for tissue engineering applications. In this study, the hybrid fibrous scaffolds of two various types of aliphatic elastomeric polyurethane (EPU) and silk fibroin (SF) were fabricated with different mass ratio by electrospinning. Physical and mechanical properties of these scaffolds were evaluated using scanning electron microscopy, attenuated total reflectance Fourier transform infrared spectroscopy, X-ray diffraction, contact angle measurement, atomic force microscopy and tensile strength analysis. Viability and attachment of human foreskin fibroblasts on the scaffolds were also assessed by MTT assay, hematoxylin-eosin and fluorescent staining and SEM. The results showed that in both types of polyurethane, by increasing the percentage of fibroin to polyurethane, the fibers diameter decreased and the uniformity of their diameter increased. Unexpected ultrafine fibers and nanowebs were seen throughout the usual fibers of EPU/SF hybrid scaffolds. Thus, the efficiency of the homing and proliferation of the fibroblasts cells onto the scaffolds was improved. Based on our results, the EPU/SF hybrid scaffolds characteristics, especially morphology, mechanical properties and biocompatibility were tunable by altering the ratio and the type of EPU. These features make these adjustable hybrids as suitable scaffolds for reconstitution of a wide range of organs such as skin, liver, uterus, esophagus, vasculature, tracheal cartilage, neurons and others.

1. Introduction

Nanostructures were found to be of a great significance because of their inherent properties such as large surface area to volume ratio and the engineered properties such as porosity, stability and permeability [1]. Development of the unique nanostructures that have almost all required properties for tissue engineering and regeneration such as (1) mimicking the structure and biological function of native extracellular matrix (ECM) that promote the adhesion of various cells, (2) good mechanical properties, (3) good biocompatibility (*in vitro* and *in vivo*), (4) adjustable biodegradability, bioabsorption and bioresorption, (5) versatile processability and tunable properties, is essential. The functionality and applicability of these nanostructures can be further improved by incorporating secondary phases resulting in the hybrid nanostructures. Hybrid biomaterials have recently been emerged as effective structures for tissue engineering scaffolds and medical prosthetic devices and implants [2,3]. Different natural (chitosan, collagen, gelatin and silk fibroin) and synthetic materials (poly L-lactic acid, poly caprolactone (PCL), polyurethane and poly lactic-co-glycolic acid) are incorporated through phase separation, self-assembly [4], gas foaming, 3D printing [5] and electrospinning [6] techniques for this purposes. However, most of the reported hybrids are fabricated using either expensive reagents or multi-step processes. Furthermore, they cannot be applied effectively for solving most of the aforementioned problems

* Corresponding authors at: Textile Engineering Department, Faculty of Engineering, Yazd University, Yazd, Iran (M. Hadizadeh). Medical Nanotechnology and Tissue Engineering Research Center, Yazd Reproductive Sciences Institute, Shahid Sadoughi University of Medical Sciences, Yazd, Iran (H. Nikukar).
E-mail addresses: hadizadeh@yazd.ac.ir (M. Hadizadeh), habibnik@ssu.ac.ir (H. Nikukar).

https://doi.org/10.1016/j.eurpolymj.2019.109294
Received 26 June 2019; Received in revised form 17 August 2019; Accepted 7 October 2019
Available online 09 October 2019
0014-3057/

regarding tissue regeneration. Therefore, development of a unique nanostructure using facile and economic fabrication technology and its widespread application can address all the aspects of tissue engineering and regeneration.

Considerable efforts to develop scaffolds for tissue engineering have been devoted using biodegradable and biocompatible polymers over the last decade. Principally, scaffold should be designed by mimicking the structure and biological function of native ECM proteins, which provide mechanical support and regulates cell activities, incorporating physical, chemical, and biological characteristics to guide cells into functional tissues via cell migration, adhesion, and differentiation. The native ECM is a molecular complex containing proteins and polysaccharides [7].

Recently, many studies have combined natural and synthetic polymers to form hybrid scaffolds using different methods to take advantages of the positive aspects of the various materials [8]. In the current study, among all of the potent polymers, natural silk fibroin extracted from silkworm cocoons (*Bombyx mori*) and synthetic elastomeric polyurethane (EPU) were applied using the electrospinning method to investigate scaffolds fabrication.

As a natural protein, silk fibroin (SF) is one of the earliest natural proteins used in the past. SF derived from silkworm plays a crucial role in biomedical applications and tissue engineering, because of its several distinct biological properties including good biocompatibility [9], good oxygen and water vapor permeability, biodegradability, and minimal inflammatory reaction [10]. Silkworm cocoons are composed of over 95% of silk fibroin coated with sericin and a small amount of carbohydrates and other impurities. SF structure is mainly composed of glycine (46%), alanine (29%), serine (18%) and other kinds of amino acids [11,12]. SF consists of a light (L) chain polypeptide and a heavy (H) chain polypeptide linked together via a single disulfide bond at the C-terminus of H-chain, forming an H–L complex [7]. The well-oriented β-sheet structure of fibroin filaments with robust mechanical properties and relatively slow proteolytic degradation makes it a preferable biomaterial compared to other natural polymers. Some researchers have investigated the effects of the SF on the cell adhesion, viability and proliferation using fibroblasts and osteoblasts in cultures which revealed its positive effects [12,13]. However, from the mechanical point of view, SF electrospun fibrous scaffolds have not sufficient characteristics to meet the requirements of some applications [14].

Polyurethane (PU) is one of the synthetic candidate materials applied for implants targeting both soft and hard tissues and other medical device components [15,16]. EPU is a flexible linear polymer consisting of soft and hard segments that exhibits good strength, flexibility, resistance to tear [17], and biocompatibility [18]. Conventional EPU is non-biodegradable but a biodegradable EPU can be synthesized which its electrospun samples achieve satisfying biomechanical behaviors [19]. Also, the *in vivo* trials of the biodegradable EPU grafts show promising results with long-term potency and remodeling [19].

Nowadays electrospinning is widely used in tissue engineering for the development of various types of scaffolds due to its utilizable properties [20–22]. Electrospinning has been recognized as one of the most simple and versatile methods to produce nanofibers with diameters in the range of 50∼1000 nm [23]. Depending on the materials and process settings, this method can provide the high interconnectivity and surface areas needed for cell activity, as well as adjustable mechanical properties [24,25]. In electrospinning method, some parameters affecting fiber characteristics include: polymer solution viscosity [26], solvent properties, applied voltage, collector speed, distance between nozzle and collector [27,28], flow rate of solution [29] and the ambient conditions [30].

Researchers studied EPU and SF mixtures aiming for vascular reconstruction. It is presumed that EPU/SF hybrids had good biocompatibility, mechanical property, and potential clinical application for vascular tissue engineering [20,21].

With the mixture of EPU and SF, the blended stent can not only maintain excellent mechanical properties, but also improve the biological properties of EPU. In this study, the hybrid fibrous scaffolds of SF and two different EPU with different mass ratio were fabricated by electrospinning. Then the morphology, wettability, surface roughness, crystallinity and mechanical properties of the scaffolds were evaluated. Further, the effect of ratio of EPU/SF and the type of EPU on nanofibers biocompatibility, cell attachment and proliferation were investigated.

2. Materials and methods

All the chemicals were purchased from Sigma Aldrich/ Merk (UK) and culture media with their supplements were purchased from Invitrogen (UK), unless otherwise stated. Two medical grades aliphatic EPUs (Tecoflex® SG-80A and Carbothane® PC-3575A) which have a hardness of 72 and 70 Shore A, respectively, were kindly gifted by Mr. Dehghanizadeh.

2.1. Preparation of silk fibroin

Silk fibroin (SF) was extracted from the natural silkworm cocoons using a protocol described by Rockwood et al. [31]. In sum, the cocoons were boiled for 1 h in an aqueous Na2CO3 solution (0.5% (w/v)) and rinsed with water to remove the sericin, then dried at room temperature to obtain pure fibroin fibers. To prepare the fibroin aqueous solution, fibroin fibers were first dissolved in a 9.3 M LiBr solution at 60 °C for 5 h. The fibroin–LiBr solution was then dialyzed against distilled water for 3 days at room temperature using a cellulose membrane (MWCO 14KDa Sigma-Aldrich®) to remove the LiBr. To completely remove residual salts water was exchanged every 6 h. Then solution was freeze-dried and then dried fibroin was stored at till be used.

2.2. Fabrication of scaffolds

The EPU/SF blends were prepared from 12% (w/v) solution of the two polymers in trifluoroacetic acid (TFA), at various ratios (100/0, 90/10, 70/30, 50/50, 30/70 and 0/100). All of the mixtures were stirred at room temperature for 2 h before electrospinning. The solution was then infused through a 2.5 ml syringe attached to a programmable syringe pump into a 21-gauge metal needle. The feeding flow rate was 0.1 ml/h, the applied voltage was 18 kV using a high voltage power supply, and the humidity was maintained at 35–40%. Located 13 cm downward from the needle tip, a ground collector at speed of 300 rpm was used to collect randomly oriented fiber mats. Electrospun scaffolds were transferred to a vacuum desiccator for at least 48 h to ensure that there was not any residual solvent on the scaffold surfaces. Then, the scaffolds treated with methanol to induce the conformational transition of less ordered fibroin molecules to the β-sheet structure, which made them water-insoluble.

2.3. Scaffold characterization

2.3.1. Attenuated total reflectance Fourier transform infrared (ATR-FTIR)

ATR-FTIR spectroscopy was used to verify the compositions of the electrospun scaffolds. The range of wavenumbers of FTIR (Equinox 55, Bruker, Germany) was from 600 to 4000 cm^{-1}.

2.3.2. Scanning electron microscopy (SEM)

To study the morphology of the electrospun EPU/SF fibers, samples were sputter coated with gold and imaged with scanning electron microscopy (ZEISS® DSM 960A Oberkochen, Germany) with an accelerating voltage of 8 kV. SEM images were then analyzed using ImageJ 1.41o software to determine fiber diameter. The average diameter was determined by randomly measuring at least 100 fibers from each SEM image and is expressed as mean ± standard deviation (SD). Three random SEM images were used for each sample.

2.3.3. Wettability contact angle

To determine the wettability (or hydrophilicity) of electrospun scaffolds, the contact angle was measured by a contact angle measurement system (KRUSS® GmbH, Hamburg, Germany). The droplet size was set at 5 μL and immediately after dropping, the changes of the droplet shape was recorded using a video camera and analyzed. To confirm the uniformity of electrospun membranes, the contact angle was measured three times for different points, and an average value was calculated by statistical method.

2.3.4. X-ray diffraction (XRD)

X-ray diffraction (XRD) Spectroscopy (D/MAX-250, Rigaku, Kyoto, Japan) was used for evaluating crystal phase in the electrospun EPU/SF fibers. The sample was scanned in the range from 5° to 50°. X'Pert HighScore Plus software (PANalytical) was used for crystalline phase identification.

2.3.5. Atomic force microscopy (AFM)

The surface morphology was investigated by atomic force microscopy (AFM) on a Scanning Probe Microscope XE 70 (Multimode-8, Bruker, Billerica MA, USA).

2.3.6. Mechanical property test

Mechanical properties were tested on an Instron SANTAM-STM-20 Testing Machine, at a gauge length of 20 mm and strain rate of 3 mm/min at room temperature, and the width of the samples was 1 cm. An average value of at least three replicates for each sample was taken.

2.4. In vitro cell culture and seeding

Fibroblast cells from human neonatal foreskin (YhFF#8; passage 23, kindly were gifted from Stem Cell Biology Research Center, Yazd Reproduction Sciences Institute) were cultured in Dulbecco's modified Eagle's medium (DMEM) supplemented with 10% fetal bovine serum (FBS), and 100 mg/mL streptomycin in a 25 cm^2 cell culture flask. Cells were incubated in a 5% CO_2 at 37 °C for 6 days. Electrospun scaffolds, which were 20 μm thick on average, collected on glass cover slips and placed in a 24 well plates were sterilized under ultraviolet (UV) radiation for 30 min and washed once with PBS. Confluent fibroblast cells were detached with 0.25% trypsin containing 0.1% EDTA. Detached cells were centrifuged at 1000 rpm for 5 min, counted by dye exclusion assay using trypan blue on a hemocytometer and seeded on electrospun scaffolds at a density of 10,000 cells per well.

2.5. Cell viability assay

The 3-(4, 5-dimethylthiazol-2-yl)-2,5-diphenyltetrazolium bromide (MTT) assay is a colorimetric method that detects metabolic activity. When viable cells are exposed to yellow MTT dye for a fixed time the cells reduce the dye to a blue product that is insoluble in PBS. The cells can then be lysed, the dye liberated, and dissolved in a known quantity of solvent, and the mixture's optical absorbance read. The number of viable cells can be determined by how much of the dye is reduced in a given time.

After 1, 3 and 7 days of cell seeding in a 24-well plate, the culture medium was replaced by 400 μL of new medium, then 40 μL of MTT solution (5 mg/mL in PBS) was added to each well. After 4 h incubation at 37 °C and 5% CO2, MTT solution from each well was carefully removed and replaced by 440 μL acid-isopropanol (100 μL of 0.04 N hydrochloric acid in isopropanol) to dissolve the dark blue crystals. After a few minutes at room temperature to ensure that all crystals were dissolved, then aliquots were pipetted into a 96-well plate. Then the optical density read (560 nm, Stat Fax-2100).

2.6. Cell attachment and morphology

2.6.1. SEM

The cell–scaffold constructs were washed with PBS and fixed with 2.5% glutaraldehyde for 2 h on the day 5. The constructs were then subjected to serial dilutions of ethanol wash (50%, 70%, 90% and 100%), with each step 5 min exposure for dehydration. The scaffolds were then coated with gold and were observed under SEM.

2.6.2. Hematoxylin-eosin (H&E) staining

H&E staining was performed to stain cell nuclei and cytoplasm respectively. YhFF#8 cultured on scaffolds for 3 and 7 days and then were fixed with 2.5% glutaraldehyde for 2 h and rinsed trice with PBS for 5 min each time. The samples were first stained with Hematoxylin and rinsed once with PBS for 5 min. Then samples were treated with acid alcohol for 3 s. After rinsing with PBS, the samples were stained with eosin. The constructs were then subjected to serial dilutions of ethanol wash (5 min exposure to 50%, 70%, 90% and 100% ethanol) for dehydration. H&E staining pictures displayed cell nucleus in blue and cytoplasm in red.

2.6.3. Immunofluorescence (IF) staining

IF was done as explained elsewhere [32]. In sum, YhFF#8 cells were cultured onto the scaffolds for 7 days and then were fixed in 4% paraformaldehyde. The samples were treated with 0.1% Triton X-100 for 30 min, rinsed trice with PBS for 5 min each time, and subsequently blocked in blocking solution of 0.25 bovine serum for 30 min at RT to minimize nonspecific binding. The samples were incubated with primary antibody (FIBRONECTIN; ab6328; diluted 1:100 in PBS) overnight at 4 °C. After rinsing with PBS, it was subsequently incubated with secondary antibody (antimouse IgG conjugated with FITC; ab6785; diluted 1:100 in PBS) for 1 h at 37 °C in dark. Then 4,6-diamidino-2-phenylindole (DAPI) was used to stain the cell nuclei (blue) for 3 min in dark. After rinsing trice with PBS, preparations were covered with mounting medium (Vectashield; Vector laboratories, USA) or PBS, and examined by microscopy with phase contrast or fluorescence with appropriate excitation optics on an inverted microscope (Olympus IX-71). Experiments were performed in triplicate.

2.7. Statistical analysis

Origin 8.0 (Origin Lab Inc., USA) was applied for statistical analysis. Data are expressed as mean ± standard deviation (SD). Statistical comparisons were made by one-way ANOVA. Tukey test was used for evaluations of differences between groups. P-values less than 0.05 were considered to be significant.

3. Results and discussion

3.1. Fourier transform infrared spectroscopy (FTIR)

The purpose of using FTIR was to confirm the existence of both types of EPUs (SG-80A & PC-3575A) and fibroin in the electrospun hybrid scaffolds. FTIR spectra of EPU, SF and EPU/SF at 90/10, 70/30, 50/50 and 30/70 ratios after methanol treatment are shown in Fig. 1. The peak shifts and the variation of intensities indicate a change in the material composition. The characteristic absorption bands of fibroin appeared at 1650 cm^{-1} (amide I C═O stretching), 1528 cm^{-1} (amide II C—N stretching and N—H distortion vibration), 1237 cm^{-1} (amide III C—N stretching and N—H deformation vibration), and 3296 cm^{-1} (amine N—H stretching). The bands in the range 800–1200 cm^{-1} are characteristics of a specific polypeptide with respect to peptide bands [33,34].

The pure EPU (SG-80A) has been extensively studied using FTIR [35]. The band near 3315 cm^{-1} is due to the stretching vibration of OH groups; The bands near 2926, 2850, and 2797 cm^{-1} were assigned to

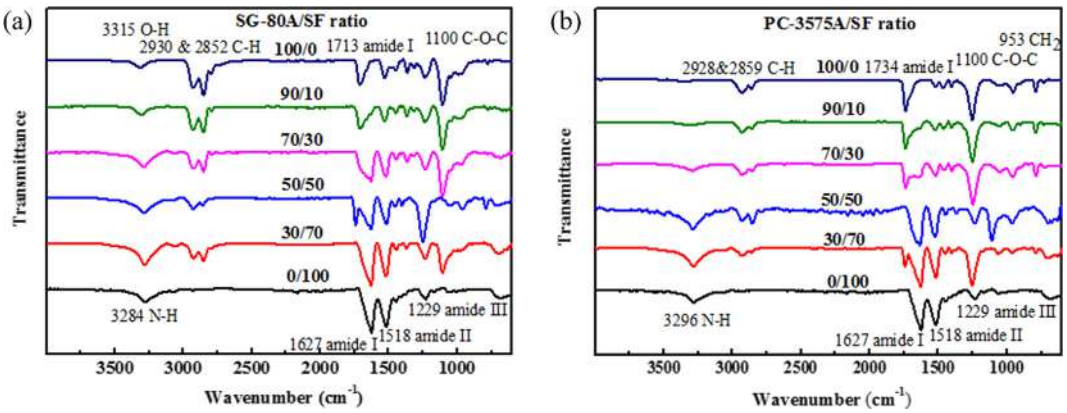

Fig. 1. ATR-FTIR spectra of EPU/SF nanofibers scaffolds with different ratios (a) SG-80A/SF, (b) PC-3575A/SF. FTIR confirmed the existence of both types of EPUs (SG-80A & PC-3575A) and SF in the electrospun hybrid scaffolds.

the asymmetric, symmetric, and CH2 stretch vibration, respectively; the band near 1713 cm^{-1} was explained by the stretching mode of (C═O) of the urethane amide I; the band near 1528 cm^{-1} was due to the stretching mode in (C—N) and (N—H) of the amide II band; the band near 1234 cm^{-1} is attributed to the stretching vibration of CO and the distorted vibration of urethane in EPU; and the band at (1110–950 cm^{-1}) is explained by the asymmetric C—O—C stretching (fatty ether). In the samples combined with SG-80A, shifts are observed at amide I and N—H groups toward 1692 cm^{-1} and 3314 cm^{-1}, respectively, indicating a change in their compositions (Fig. 1a). With the increase in the SF content, the band near 3315 cm^{-1} assigned to the stretching vibration of OH groups was shifted to 3314, 3293 and 3280 cm^{-1} in the hybrid scaffolds. Also, the presence of CH_2 symmetric stretching vibrations at 2925 and 2852 cm^{-1}, and the stretching of ether groups C—O—C at 1100 cm^{-1}, demonstrates the incorporation of SG-80A with fibroin [35]. When the content ratio of the EPU increased, the intensities of these three peaks increased obviously.

It can be observed in Fig. 1b that peaks in PC-3575A scaffold appeared at (2928 cm^{-1} and 2859 cm^{-1}), which are due to asymmetric or symmetric stretching in (C—H) in CH2. In the fingerprint region of the polymer (i.e., 1745–957 cm^{-1}), we can see the peak at 1734 cm^{-1}, which is due to the stretching mode of (C═O) of the urethane amide I. The peak at 1519 cm^{-1} appears due to the stretching mode in (C—N) and (N—H) of the amide II band. The peaks at 1462 cm^{-1} and 1404 cm^{-1} are due to bending vibrations in CH2 groups. Also, the peak positioned at 953 cm^{-1} is attributed to the in-plane CH2 bending vibration in CH2 groups [36].

All the peaks in the FTIR spectrum of SF were also observed in the FTIR spectra of EPU/SF nanofibers. This means that the characteristic peaks of EPU and SF appear in the EPU/SF nanofibers. With the increase of SF content, the characteristic peak intensity of EPU decreased, and the peak intensity of SF increased. The same absorption peaks of EPU/SF scaffolds indicate that EPU and SF will not change their molecular structure in blends.

3.2. Microstructure and morphology of fibers

SEM images indicated that the composition ratio of EPU to SF and the type of EPU play an important role in determining the nanofibrous structure and morphology (Fig. 2). In pure SG-80A and SG-80A/SF 90/10, distinct nanofibers weren't formed maybe because of insufficient solvent evaporation. While, pure PC-3575A and PC-3575A/SF 90/10 shaped obvious discrete nanofibers.

Unexpected ultrafine fibers and nanowebs were also widely distributed throughout the usual fibers of EUP/SF hybrid scaffolds. These nanowebs were web shaped ultrafine fibers with diameters under 100 nm, appeared after addition of 30% and 10% silk fibroin to SG-80A and PC-7535A respectively. Fig. 3a and b show two examples of these newfound nanowebs in SG-80A/SF and PC-3575A/SF scaffolds with 30/70 composition. A similar nanoweb structure was seen in previous research by Ding et al. on electrospun poly(-acrylic acid) (PAA) and polyamide-6 mats [37]. It is assumed that the fast phase separation of the blended polymer and solvent is the main reason for the formation of the nanowebs. The evaporation of TFA and the rapid solidification of EPU/fibroin during the electrospinning process may induce the formation of the fine porous structures. These nanowebs effectively increase the surface area and may be favorable for cell attachment and spreading.

The average diameter of SG-80A, PC-3575A and SF fibers alone were 727 ± 416, 326 ± 172 and 216 ± 190 nm respectively. By adding SF to the mentioned EPUs, the fibers had lower diameters and higher uniformity especially about SG-80A ($P < 0.05$) (Fig. 3c and d). SF is a typical amphoteric polymer electrolyte, consisting of highly repeating amino acids such as glycine and alanine and a large side chain containing a charged amino acid. When SF was added to the spinning solution, the charge density of the solution increases, which enhances the electrostatic force on the electrodes and the elongational force applied to the electrospinning jet, leading to the generation of fine fibers [25,38]. The formation of the fine nanofibers is considered to be due to increased conductivity of the final solution. Followed by a methanol treatment, the fibroin in the hybrid scaffold became water-insoluble. After methanol treatment, the fibers swelled and changed to a crimped structure, which was regarded as the effects of retraction of the elongated polymer chains in each fiber [39]. Furthermore, the shrinkage effect caused the fibers to develop a crimped structure that mimicked the wavy structure of natural collagen fibers.

3.3. Hydrophilicity

The surface wettability is mandatory for cell attachment to scaffolds for most of the body cells that led to cell migration, proliferation and survival [40], and can be measured with water droplet contact angle. In order to increase hydrophilicity, adding naturally derived hydrophilic polymers into synthetic polymers would be an efficient approach [41].

SF has many hydrophilic groups, such as amine and carboxyl moieties, and the less hydrophilicity of EPUs (SG-80A and PC-3575A) can be attributed to their aliphatic polyether structures. Fig. 4 shows the water droplet contact angles for electrospun EPU, SF and EPU/SF scaffolds. The contact angle values for pure SG-80A, PC-3575A and SF were 90° ± 0°, 88.6° ± 5° and 56° ± 6°, respectively ($P < 0.05$). However, it is noteworthy that the decline was not as remarkable as we expected. The possible reason is that ethanol treatment resulted in the increase of parallel folding crystalline structure of SF in the scaffolds, which weakened the hydrophilicity. After combination of SF with both

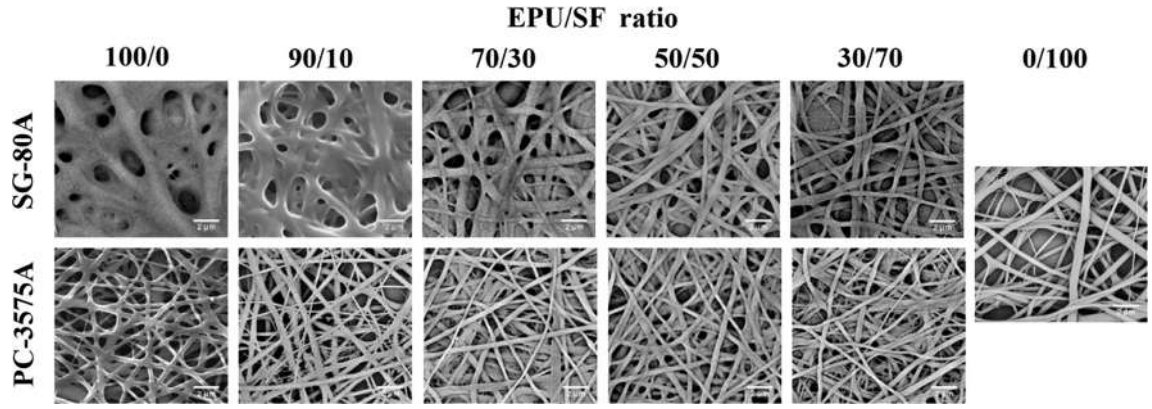

Fig. 2. SEM images of the methanol-treated electrospun fibers. Scale bar 2 μm.

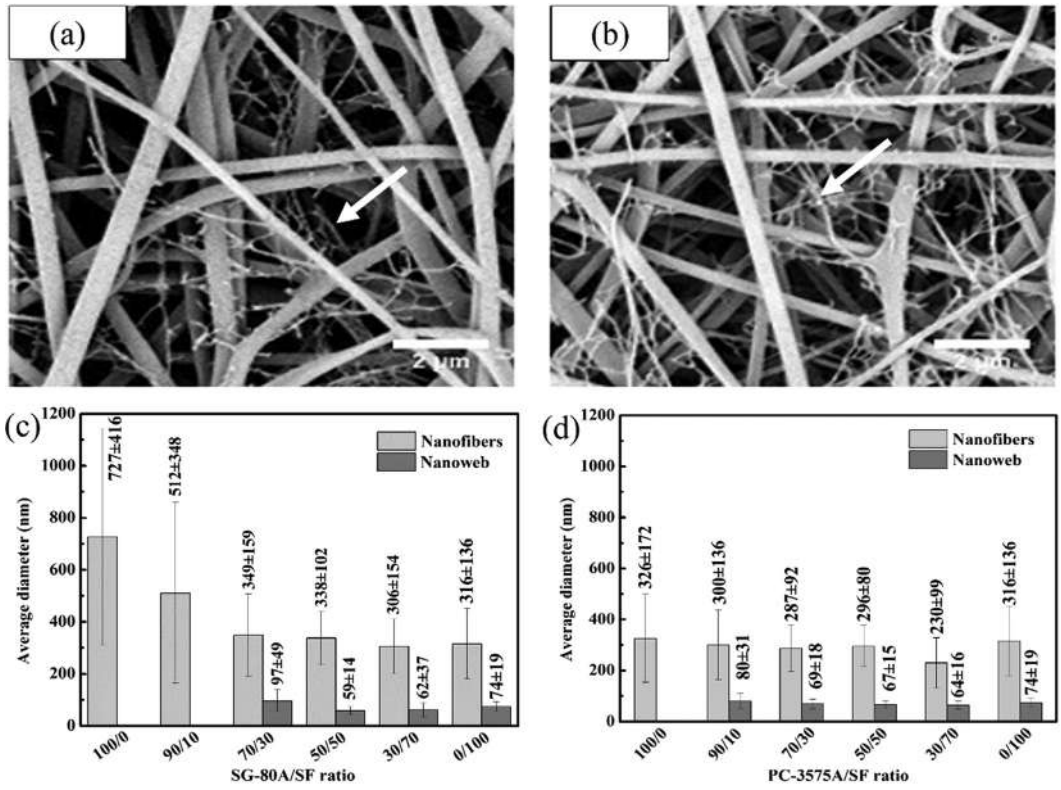

Fig. 3. Ultrafine nanofibers and nanowebs distributed within the electrospun samples (a) SG-80A/SF 30/70, (b) PC-3575A/SF 30/70. Arrows represent nanowebs distribution throughout the usual nanofibers of EUP/SF hybrid scaffolds. Scale bar 2 μm. (c, d) nanofibers and nanowebs diameter graphs of the methanol-treated electrospun fibers. By adding SF to the mentioned EPUs, the fibers had lower diameters and higher uniformity.

of the EPUs, water droplets were absorbed more quickly onto the scaffolds than they were with the EPU alone. At EPU/SF ratio of 90/10 for both EPUs, contact angle had a fast decline to 76.5° and 75.6° respectively. The more SF percent increased, the more hydrophilicity raised, but by a slower slope. The hydrophilicity of the EPU/SF electrospun scaffold ensured that they could be used successfully for cell seeding. The contact angle results showed that the hydrophilicity of PC-3575A/SF scaffolds was more than SG-80A/SF scaffolds. The increase in contact angle was not conducive to the rapid wetting of the material on the surface and the rapid cell adhesion [42]. However, if extend the infiltration time, when the scaffold was completely wetted by the liquid, the larger surface area of the hydrophobic material surface would provide more sites for cell adhesion. Totally, surface wettability of the most hybrid nanofibrous scaffolds tend to be hydrophilic, and would be suitable for cells adhesion and proliferation.

3.4. X-ray diffraction

Crystal structure of polymers plays an important role in hydrophilicity and cellular behavior on the surface of scaffolds. For this reason, XRD analysis was performed to measure the degree of crystallinity. The XRD patterns of EPU/SF hybrid scaffolds exhibited the characteristic peaks related to EPUs and SF (Fig. 5). The crystallinity of hybrid polymers with the weight ratio from 100/0 to 0/100 was 45%, 39%, 40%, 38%, 37% and 40% for SG-80A/SF and 57%, 58%, 47%, 41%, 36% and 40% for PC-3575A/SF scaffolds, showing a decreasing manner with the increase of SF content. SF can hinder the formation of EPU crystalline structure. In the XRD patterns of EPU/SF blend scaffolds, diffraction peaks at near 17°, 22° and 23° were observed for all samples, but the area under the diffraction peaks was different (Fig. 5). The pure SG-80A scaffold had a lower peak area than pure PC-3575A scaffold. This increase in the diffraction peak area, means the higher

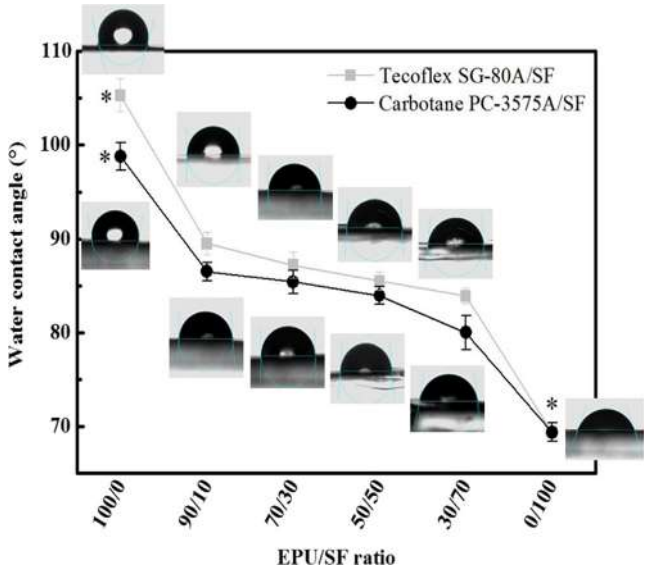

Fig. 4. Evaluation of wettability of EPU, SF and EPU/SF electrospun scaffolds by contact angle measurement. By increases in SF ratio, a decreasing pattern in contact angle (increase in hydrophilicity) has been shown. Results are expressed as mean ± SD (*P < 0.05).

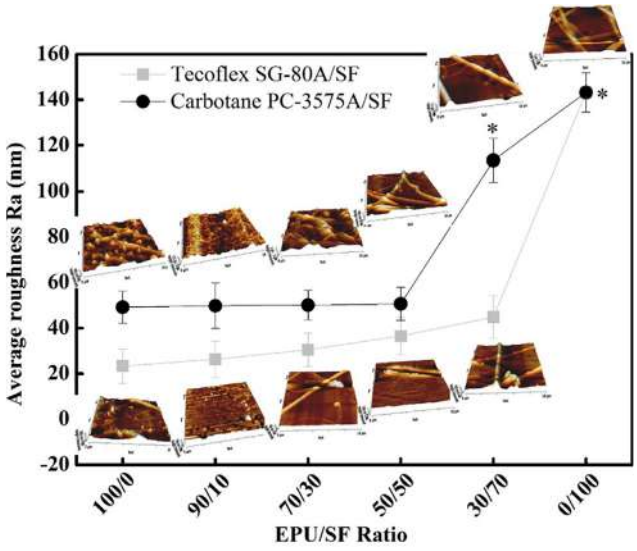

Fig. 6. Quantitative AFM analysis: mean roughness Ra and 3D images of the surfaces of EPU, SF and EPU/SF electrospun scaffolds. Analyzed area equals to $10 \times 10\,\mu m^2$. An increasing trend in average roughness by increases in SF concentration was noted. Results are expressed as mean ± SD (*P < 0.05).

crystallinity degree and the higher molecular orientation of pure PC-3575A.

The beaded fibers of SG-80A polymer may be correspond to low crystallinity degree and molecular orientation, and the PC-3575A fibers even diameter possibly correlated to its high crystallinity degree. The intensity of the peak at 17.2° corresponding to SF became strong with the increase of SF content in EPU/SF blends, while the intensity of peak at near 22° and 23° related to EPU became weak. Therefore, SF can change the crystallinity and wettability of hybrid scaffolds. The crystalline region of EPUs and SF is compatible with each other, which reduces the possibility of phase separation. Previous studies demonstrated that amorphous surfaces were suitable for cell attachment and proliferation than highly crystalline surfaces [43]. This might be the reason for showing good cellular attachment and proliferation in EPU/SF electrospun scaffolds.

3.5. Surface morphology and roughness

The surface properties of the EPU/SF scaffolds were studied by three-dimensional (3D) AFM images. The surface roughness of pure EPUs, shown as Ra, was lower than for the blended EPU/SF scaffolds, suggesting that blending SF with EPUs resulted in an increase in surface roughness (Fig. 6). The Ra of the SF scaffold was 143 nm, which was the highest among all scaffolds. Therefore, the roughness of pure SF nanofibers was significantly high (P < 0.05). The pure SG-80A compared to the pure PC-3575A, had a smoother surface (Fig. 6). The roughness of the SG-80A/SF blended scaffolds was lower than the PC-3575A/SF scaffolds too. The roughness measured by the AFM depends on the size of the area selected. In this work, the area was kept constant, $10 \times 10\,\mu m^2$, for all measurements. The roughness value reported here is the arithmetic average of the deviations of height from the central horizontal plane, given in terms of millivolts of the measured current and is calculated using the Nanoscope Image Processing software (VECCO). It is reported that a rough surface provides greater cell attachment and a greater proliferation environment [44].

3.6. Mechanical properties

Fig. 7 shows ultimate tensile strength, elongation-at-break and Young's modulus of electrospun fibers of SF, SG-80A, PC-3575A and their blends.

SG-80A is a soft EPU possessing an intrinsically lower tensile strength and Young's modulus than PC-3575A. In contrast, the PC-3575A had the lowest strain strength. Compared to the two EPUs, SF

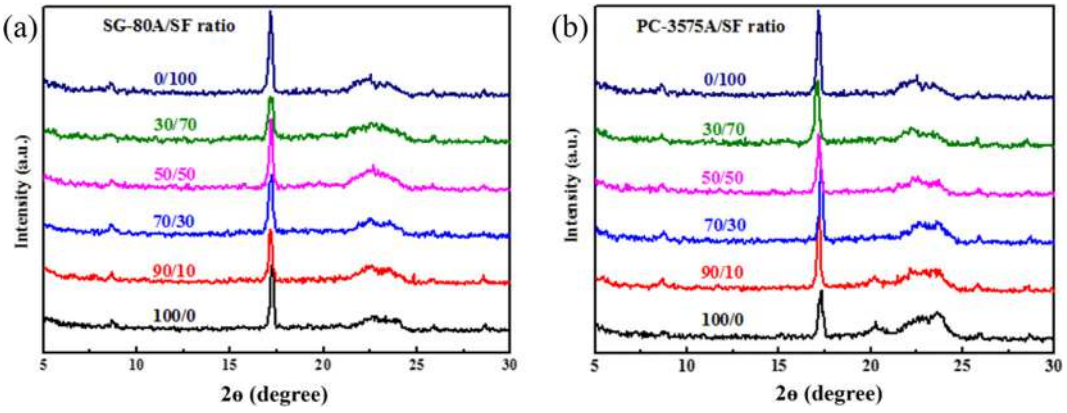

Fig. 5. X-ray diffraction patterns of ethanol-treated electrospun EPU, SF and EPU/SF nanofibers scaffolds with various weight ratio: (a) SG-80A/SF, (b) PC-3575A/SF. Due to the XRD patterns of scaffolds, a with the increase of SF content decreased the area under the peaks (crystallinity).

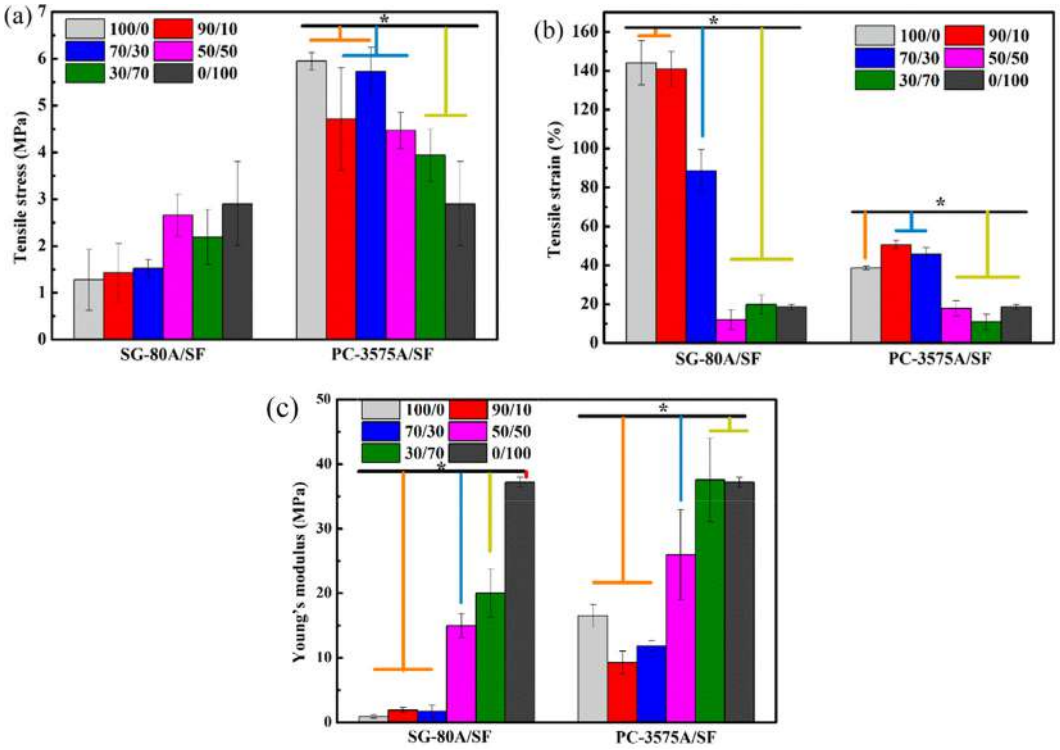

Fig. 7. Mechanical properties of various EPU/fibroin blends including representative (a) Tensile strengths values, (b) Elongation-at-break values and (c) Young's modules values. Results are expressed as mean ± SD (*P < 0.05). Composition ratio of EPU to SF and the type of EPU were important factors in determining the nanofibers mechanical properties.

had higher Young's modulus. Our results exhibited these differences distinctly. These findings show that SF has suitable mechanical strength while SG-80A has poor strength but good elasticity. When SF and SG-80A were mixed and electrospun together, it can be seen that adding fibroin, effectively reinforced the strength and Young's modulus of the hybrid up to 50/50 ratio. Raising SF proportion over 50%, reduced the ductility of SF/SG-80A mixture. The lower strain of the SG-80A/SF (30/70) sample could be contributed to fibroin brittleness; namely, the lower extensibility that hindered it from being stretched farther. Consequently, the SG-80A/SF (70/30) sample displayed both favorable strength and strain properties.

PC-3575A scaffold exhibited the highest ultimate tensile strength. There was an obvious increase in the strain to maximum with the raise of SF content in PC-3575/SF (90/10) blend. Thus, PC-3575A/SF (90/10 & 70/30) displayed the highest strain and had favorable strength (Fig. 7a and b).

When the mass ratio of PC-3575A to SF decreased from 70/30 to 30/70, Young's modulus obviously increased while tensile strain clearly declined.

Above results confirmed that the SF electrospun fibers could not meet the required fracture resistance needed for tissue engineering applications [16]. But, blended EPU/SF electrospun fiber scaffolds by taking the advantage of good mechanical properties of the EPU synthetic polymers brought good biocompatibility and mechanical properties from both polymers [20].

As shown in Table 1, with respect to reported mechanical properties of some human normal tissues and organs, it is possible to use the SG-80A/SF 70/30 for engineering the soft tissues such as liver [45,46]. SG-80A/SF 90/10, 30/70 and PC-3575A/SF 50/50 have sufficient tensile strength, elongation-at-break and Young's modulus for tissue engineering and regeneration of human skin tissue [47–49] which needs more resistance and elasticity. While, SG-80A/SF 70/30, PC-3575A/SF 90/10, 70/30 and SG-80A/SF 50/50, 30/70 have acceptable similarities to the human uterus, vagina and bladder tissues [50–52,59]. Surprisingly, some blends of our selected polymers have the adequate mechanical properties for engineering of vascular, esophageal and tracheal cartilage (SG-80A/SF 90/10, SG-80A/SF 50/50, 30/70 and PC-3575A/SF 90/10, 70/30) [53–57]. In addition to the various mentioned possible applications, the PC-3575A/SF 90/10 and 70/30 blends may be used as promising scaffolds for reconstruction of peripheral nerves [58].

3.7. Viability and proliferation of YhFF#8 cells on the hybrid scaffolds

In order to determine cell response to prepared nanofibrous scaffolds, YhFF#8 were seeded onto the scaffolds and then cell proliferation was evaluated by MTT assay at days 1, 5 and 7. Glass coverslips without any electrospun scaffold were used as control. As shown in Fig. 8, proliferation increased along with the culture time, indicating cell proliferation proceeded normally.

At day 1, absorbance at 570 nm did not have significant difference in all scaffold groups, indicating that the cells had adapted to the culture bed. However, at days 5 and 7, cell proliferation in the pure EPU scaffolds was evidently lower than other groups. These results demonstrated that the scaffolds containing SF could promote cell adhesion and proliferation in agreement with previous studies [20,60]. Consequently, by increasing SF proportion, YhFF#8 displayed an exponential increase in cell population density on EPU/SF scaffolds after 7 days culture, with the highest rate of proliferation for EPU/SF 30/70 scaffolds ($P < 0.05$). PC-3575A had better supporting behavior in cell spreading and proliferation at all ratios than SG-80A, maybe due to lower diameter and architecture of its hybrid nanofibers.

3.8. Cell attachment, morphology and growth on nanohybrid scaffolds

To assess the biocompatibility and the capability of the scaffolds for tissue engineering applications, YhFF#8 cells were plated onto the scaffolds. The *in vitro* cytocompatibility study showed that the

Table 1
Mechanical properties of some normal tissues with their proposed mimicry scaffolds.

Tissue type	Stress at failure (MPa)	Strain at failure (%)	Modulus (MPa)	Suggested scaffold	Study
Liver	0.047 ± 0.025	27–37	0.35–0.79	*SG-80A/**SF 70/30	Chen et al. [45] Kemper et al. [46]
Human abdomen, skin	1.0–24.0	100–300	0.1	SG-80A/SF 90/10	Jansen and Rottier [47] Dunn and Silver [48]
Human leg, skin	–	–	6–22	*PC-3575A/SF 50/50, SG-80A/SF 30/70	Manschot [49]
Uterus	0.17–1.14	21–43	–	SG-80A/SF 70/30	Manoogian et al. [50]
Vagina	0.82–2.62	20–46	2.5–9.5	SG-80A/SF 50/50 PC-3575A/SF, 90/10, 70/30	Rubod et al. [51]
Bladder	0.5–2.6	–	1–4.1	SG-80A/SF 50/50, 30/70	Martins et al. [52]
Vascular: saphenous vein	1.02–1.28	–	0.85–0.91	SG-80A/SF 90/10	Centola et al. [53] L'Heureux et al. [54]
Vascular: carotid arteries	1.76–2.64	110–200	–	SG-80A/SF 90/10	Kurane et al. [55]
Esophagus	1.16–2.84	–	–	SG-80A/SF 50/50, 30/70	Yu et al. [56]
Tracheal cartilage	3.5–4	Up to 50	12.17–20.54	PC-3575A/SF 90/10, 70/30	Safshekan et al. [57]
Peripheral nerve	3.51–5.93	50–100	8.45–16.67	PC-3575A/SF 90/10, 70/30	Ju et al. [58]

* Elastomeric polyurethane.
** Silk fibroin

nanohybrid scaffolds fabricated in this study were not toxic to YhFF#8 cells. Cell attachment and proliferation among the EPU, EPU/SF and SF scaffolds visualized using SEM, H&E and immunofluorescence staining. Microscopic data showed that fibroblasts attached and spread over the entire scaffolds surface (Figs. 9–11). It was revealed that cell attachment and growth within the scaffolds is depended to the fibers diameter and mechanical properties. Integration of EPUs with SF not only changed the mean fiber diameter of the scaffolds [20,60], but also improved their mechanical properties. The more fibroin added the higher attachment and proliferation rates was observed after seven days in H&E micrographs (Fig. 9).

As indicated in SEM micrographs (Fig. 10), fibroblasts attached and generated an extensive network of cells after 5 days on the hybrid scaffolds especially in the case of PC-3575A. Morphologically, the cells on these contexts looked bigger, flatter, and attached more firmly to the scaffolds.

IF staining for EPU/SF 30/70 scaffold as our optimal cell growth bed, with DAPI and FIBRONECTIN antibodies, also confirmed the mentioned data from SEM and H&E staining (Fig. 11). These results were completely consistent with the results observed in viability studies (Fig. 8).

3.9. Conclusion

In this study, a novel hybrid scaffold composing two different types of aliphatic elastomeric polyurethane (EPU) and silk fibroin (SF) with different mass ratios were fabricated by electrospinning. The nanofibrous scaffolds were evaluated via morphology, wettability, surface roughness, crystallinity and mechanical analysis. These properties could be adjusted by changing the ratio of EPU/SF and the type of EPU. It has been already, demonstrated that both of the mechanical properties and the structural features of electrospun scaffolds are key factors in cell proliferation. By adding SF to the both types of EPUs, the fibers had lower diameters and higher uniformity with increased proportion of ultrafine nanowebs. Surface wettability and roughness were also increased.

Two EPUs exhibited very distinct manners after fusion with SF. EPU (PC-3575A) had high tensile strength against low strain strength. There was an obvious increase in the strain to maximum with the raise of SF content in PC-3575/SF (90/10) blend. When the mass ratio of PC-3575A to SF decreased from 70/30 to 30/70, Young's modulus obviously increased while tensile strain clearly declined. EPU (SG-80A) has poor strength but good elasticity. Adding fibroin effectively reinforced the strength and Young's modulus of the hybrid.

The biocompatibility of all hybrid scaffolds in contact with YhFF#8 for 1, 5 and 7 days was confirmed. The more fibroin added the higher attachment and proliferation rates was observed compared to pure EPUs or SF. Cell spreading and proliferation on all concentrations of PC-3575A/SF was superior to SG-80A/SF perhaps due to more nanowebs formation, hydrophilicity, roughness and proper mechanical characteristics that make it more supportive environment for cell growth. Our results indicated that, incorporation of EPU and SF, not only possessed superior mechanical properties, moderate surface wettability and good roughness, but also promoted the proliferation, adhesion,

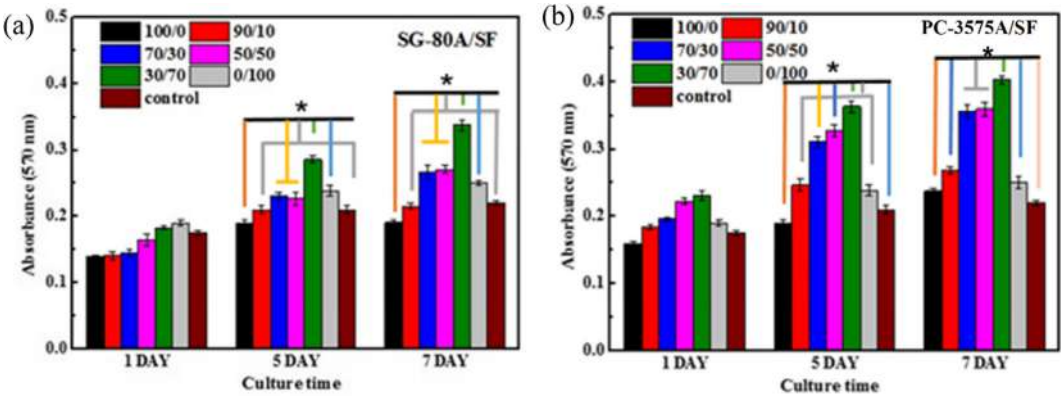

Fig. 8. Viability and proliferation of EPU, SF and EPU/SF scaffolds. In both of EPU (a) SG-80A/SF, (b) PC-3575A/SF, the more SF percent increased cells viability and proliferation. Glass coverslips without any electrospun scaffold were used as control. Results are expressed as mean ± SD (*P < 0.05).

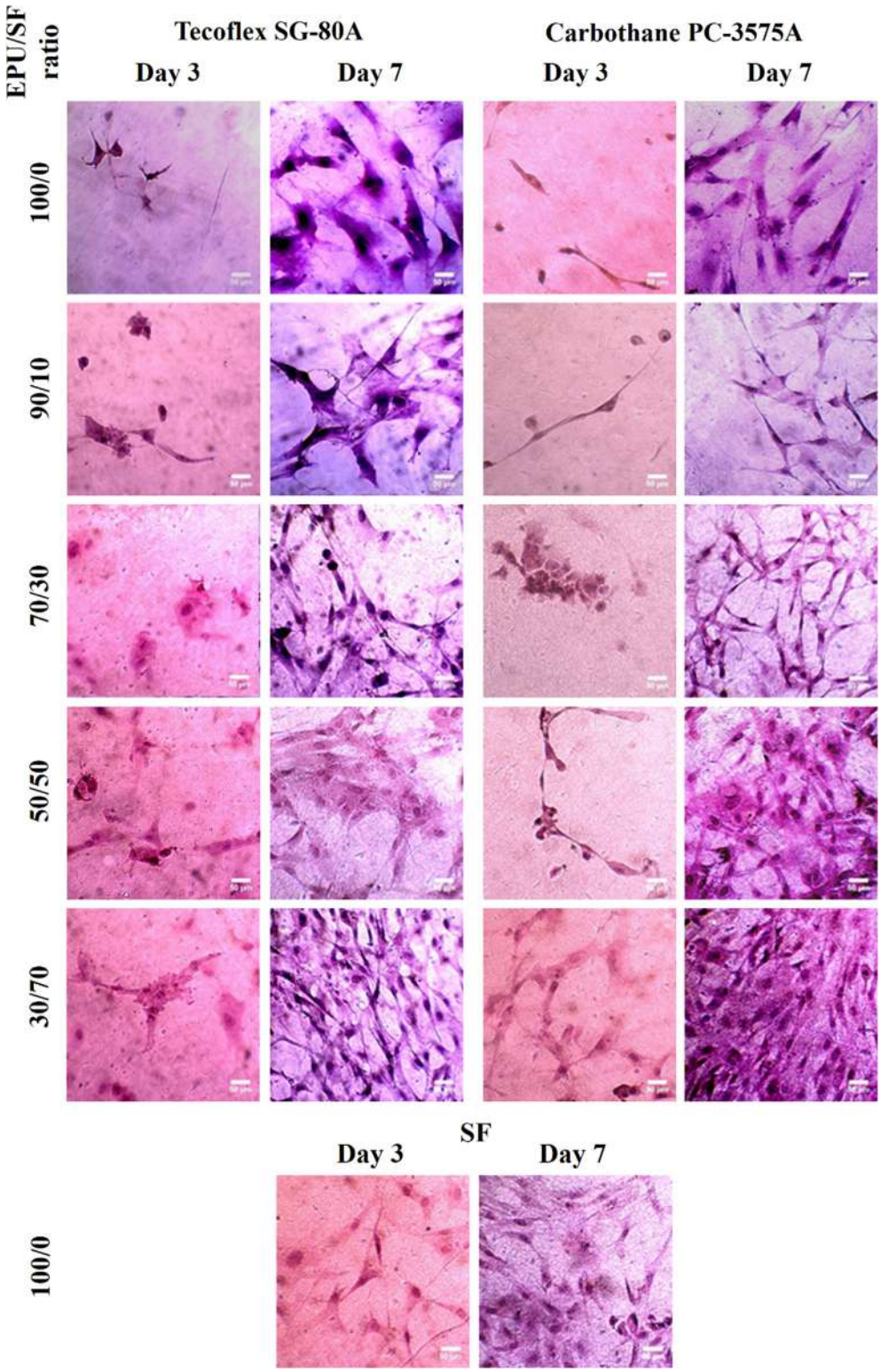

Fig. 9. H&E staining micrographs of YhFF#8 cultured on scaffold for 3 and 7 days. In both of EPU, the highest cells proliferation were in EPU/SF 30/70 scaffolds especially in the case of PC-3575A. Scale bar 50 μm.

spreading.

Surprisingly, versatile mechanical properties of some blends of our selected polymers suited them for engineering of variety of tissues from vascular, esophageal and tracheal cartilage to peripheral nerves. These data introduce the electrospun EPU/SF hybrid nanofibrous scaffolds as promising potential tools for a wide range of tissue engineering applications.

Declaration of Competing Interest

The authors declare that they have no conflict of interest in the data presented in this manuscript.

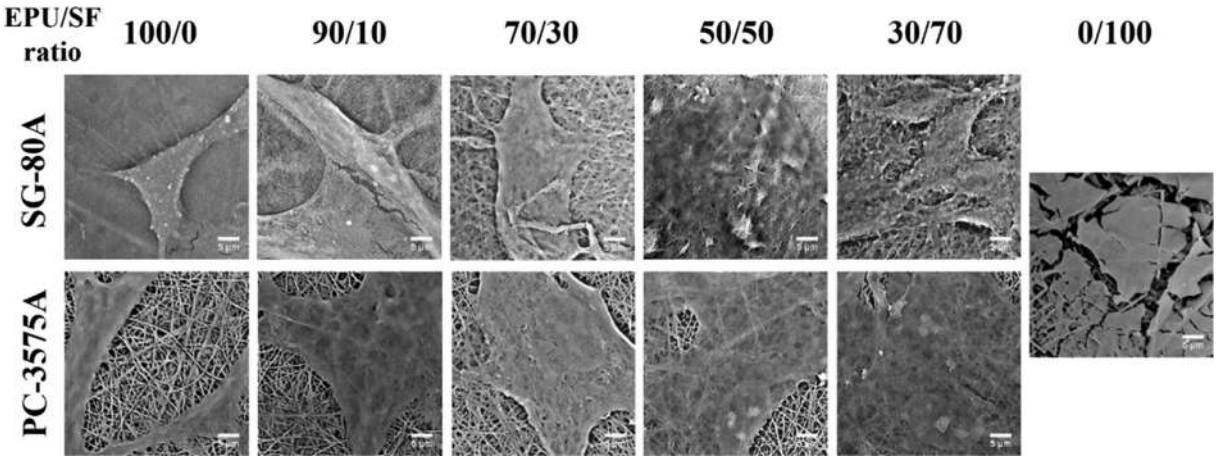

Fig. 10. SEM micrographs of YhFF#8 cultured on EPU/SF hybrid scaffolds after 5 days. Scale bar 5 μm.

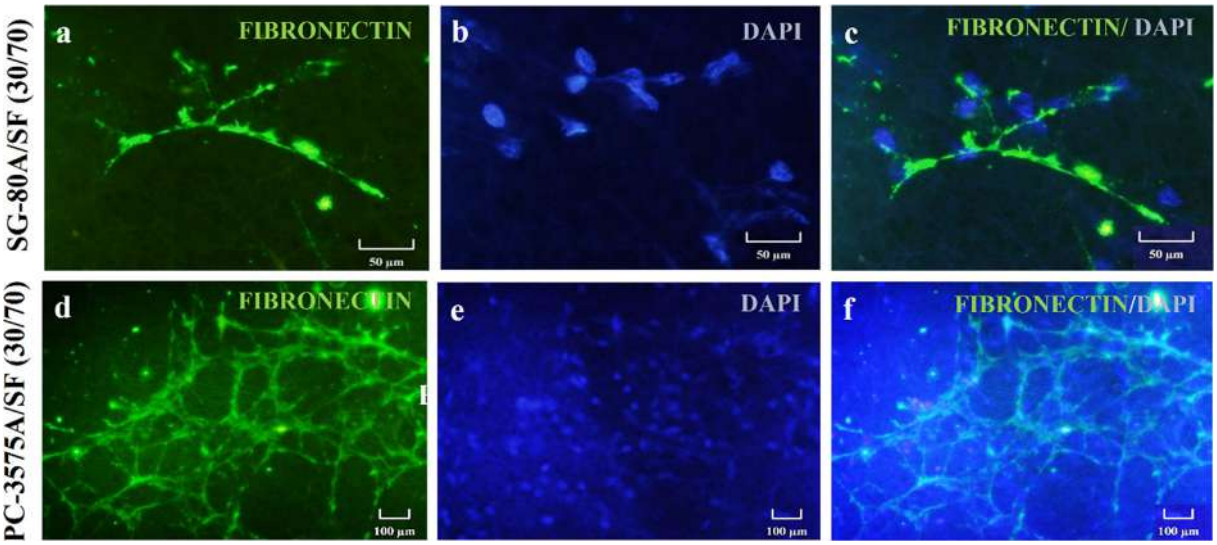

Fig. 11. Immunofluorescence images shows cell attachment and proliferation on (a, b, c) SG-80A/SF and (d, e, f) PC-3575A (30/70) scaffolds after 7 days. Green: FIBRONECTIN, Blue: DAPI. (For interpretation of the references to colour in this figure legend, the reader is referred to the web version of this article.)

Acknowledgments

The authors would like to thank the Iran National Science Foundation (INSF; Project no. 96004640), Yazd University Research Council and Yazd Reproductive Sciences Institute (Grant no. 5660) for their financial support. We are grateful to Hossein Mollahosseini, Fatemeh Sadeghian-Nodoushan, Fatemeh Akyash and Jalal Golzadeh for their cooperation and technical support.

Appendix A. Supplementary material

Supplementary data to this article can be found online at https://doi.org/10.1016/j.eurpolymj.2019.109294.

References

[1] M.J. Biggs, R.G. Richards, M.J. Dalby, Nanotopographical modification: a regulator of cellular function through focal adhesions, Nanomedicine 6 (2010) 619–633, https://doi.org/10.1016/j.nano.2010.01.009.

[2] M.S. Scholz, J.P. Blanchfield, L.D. Bloom, B.H. Coburn, M. Elkington, J.D. Fuller, M.E. Gilbert, S.A. Muflahi, M.F. Pernice, S.I. Rae, The use of composite materials in modern orthopaedic medicine and prosthetic devices: A review, Compos. Sci. Technol. 71 (2011) 1791–1803, https://doi.org/10.1016/j.compscitech.2011.08.017.

[3] E. Salernitano, C. Migliaresi, Composite materials for biomedical applications: a review, J. Appl. Biomater. Biomech.. 1 (2003) 3–18, https://doi.org/10.1177/228080000300100102.

[4] T. Weigel, G. Schinkel, A. Lendlein, Design and preparation of polymeric scaffolds for tissue engineering, Expert Rev. Med. Devices 3 (2006) 835–851, https://doi.org/10.1586/17434440.3.6.835.

[5] S. Yang, K.F. Leong, Z. Du, C.K. Chua, The design of scaffolds for use in tissue engineering. Part II. Rapid prototyping techniques, Tissue Eng. 8 (2002) 1–11, https://doi.org/10.1089/107632702753503009.

[6] H. Li, Y. Xu, H. Xu, J. Chang, Electrospun membranes: control of the structure and structure related applications in tissue regeneration and drug delivery, J. Mater. Chem. B 2 (2014) 5492–5510, https://doi.org/10.1039/C4TB00913D.

[7] H.S. Nalw, Handbook of Nanostructured Biomaterials and Their Applications in Nanobiotechnology Vol. 2 American Scientific Publishers, 2007.

[8] V. Catto, S. Farè, G. Freddi, M.C. Tanzi, Vascular tissue engineering: recent advances in small diameter blood vessel regeneration, ISRN Vascular Med. (2014) 1–27, https://doi.org/10.1155/2014/923030.

[9] Y. Feng, X. Li, M. Li, D. Ye, Q. Zhang, R. You, W. Xu, Facile preparation of biocompatible silk fibroin/cellulose nanocomposite films with high mechanical performance, ACS Sustain. Chem. Eng. 5 (2017) 6227–6236, https://doi.org/10.1021/acssuschemeng.7b01161.

[10] W. Zhou, Z. Jia, P. Xiong, J. Yan, Y. Li, M. Li, Y. Cheng, Y. Zheng, Bioinspired and biomimetic AgNPs/gentamicin-embedded silk fibroin coatings for robust antibacterial and osteogenetic applications, ACS Appl. Mater Interfaces. 9 (2017) 25830–25846, https://doi.org/10.1021/acsami.7b06757.

[11] J. Brown, C.L. Lu, J. Coburn, D.L. Kaplan, Impact of silk biomaterial structure on proteolysis, Acta Biomater. 11 (2015) 212–221, https://doi.org/10.1016/j.actbio.2014.09.013.

[12] K. Cai, K. Yao, Y. Cui, Z. Yang, X. Li, H. Xie, T. Qing, L. Gao, Influence of different surface modification treatments on poly(D, L-lactic acid) with silk fibroin and their effects on the culture of osteoblast in vitro, Biomaterials 23 (2002) 1603–1611, https://doi.org/10.1016/S0142-9612(01)00287-3.

[13] K. Cai, K. Yao, S. Lin, Z. Yang, X. Li, H. Xie, T. Qing, L. Gao, Poly(D, L-lactic acid)

surfaces modified by silk fibroin: effects on the culture of osteoblast in vitro, Biomaterials 23 (2002) 1153–1160, https://doi.org/10.1016/S0142-9612(01)00230-7.
[14] F. Zhou, X. Zhang, D. Cai, J. Li, Q. Mu, W. Zhang, S. Zhu, Y. Jiang, W. Shen, S. Zhang, H.W. Ouyang, Silk fibroin-chondroitin sulfate scaffold with immuno-inhibition property for articular cartilage repair, Acta Biomater. 63 (2017) 64–75, https://doi.org/10.1016/j.actbio.2017.09.005.
[15] R.J. Zdrahala, I.J. Zdrahala, Biomedical applications of polyurethanes: a review of past promises, present realities, and a vibrant future, J. Biomater. Appl. 14 (1999) 67–90, https://doi.org/10.1177/088532829901400104.
[16] L.P. Gabriel, A.A. Rodrigues, M. Macedo, A.L. Jardini, Filho R. Maciel, Electrospun polyurethane membranes for Tissue Engineering applications, Mater. Sci. Eng. C Mater. Biol. Appl. 72 (2017) 113–117, https://doi.org/10.1016/j.msec.2016.11.057.
[17] D.W. Park, S.H. Ye, H.B. Jiang, D. Dutta, K. Nonaka, W.R. Wagner, K. Kim, In vivo monitoring of structural and mechanical changes of tissue scaffolds by multi-modality imaging, Biomaterials 35 (2014) 7851–7859, https://doi.org/10.1016/j.biomaterials.2014.05.088.
[18] P.A. Nair, P. Ramesh, Electrospun biodegradable calcium containing poly(ester-urethane)urea: synthesis, fabrication, in vitro degradation, and biocompatibility evaluation, J. Biomed. Mater. Res. A 101 (2013) 1876–1887, https://doi.org/10.1002/jbm.a.34490.
[19] H. Bergmeister, N. Seyidova, C. Schreiber, M. Strobl, C. Grasl, I. Walter, B. Messner, S. Baudis, S. Frohlich, M. Marchetti-Deschmann, M. Griesser, M. di Franco, M. Krssak, R.H.S. Lisk, Biodegradable, thermoplastic polyurethane grafts for small diameter vascular replacements, Acta Biomater. 11 (2015) 104–113, https://doi.org/10.1016/j.actbio.2014.09.003.
[20] J. Du, T. Zhu, H. Yu, J. Zhu, C. Sun, J. Wang, S. Chen, J. Wang, X. Guo, Potential applications of three-dimensional structure of silk fibroin/poly (ester-urethane) urea nanofibrous scaffold in heart valve tissue engineering, Appl. Surf. Sci. 447 (2018) 269–278, https://doi.org/10.1016/j.apsusc.2018.03.077.
[21] E. Yu, J. Zhang, J.A. Thomson, L.S. Turng, Fabrication and characterization of electrospun thermoplastic polyurethane/fibroin small-diameter vascular grafts for vascular tissue engineering, Int. Polym. Process. 31 (2016) 638–646, https://doi.org/10.3139/217.3247.
[22] P. Sagitha, C. Reshmi, S.P. Sundaran, A. Sujith, Recent advances in post-modification strategies of polymeric electrospun membranes, Eur. Polym. J. 105 (2018) 227–249, https://doi.org/10.1016/j.eurpolymj.2018.05.033.
[23] M. Kitsara, O. Agbulut, D. Kontziampasis, Y. Chen, P. Menasche, Fibers for hearts: A critical review on electrospinning for cardiac tissue engineering, Acta Biomater. 48 (2017) 20–40, https://doi.org/10.1016/j.actbio.2016.11.014.
[24] A. Hasan, A. Memic, N. Annabi, M. Hossain, A. Paul, M.R. Dokmeci, F. Dehghani, A. Khademhosseini, Electrospun scaffolds for tissue engineering of vascular grafts, Acta Biomater. 10 (2014) 11–25, https://doi.org/10.1016/j.actbio.2013.08.022.
[25] Q.P. Pham, U. Sharma, A.G. Mikos, Electrospinning of polymeric nanofibers for tissue engineering applications: a review, Tissue Eng. 12 (2006) 1197–1211, https://doi.org/10.1089/ten.2006.12.1197.
[26] R.M. Nezarati, M.B. Eifert, E. Cosgriff-Hernandez, Effects of humidity and solution viscosity on electrospun fiber morphology, Tissue Eng. Part C: Methods 19 (2013) 810–819, https://doi.org/10.1089/ten.tec.2012.0671.
[27] T.B. Bini, S. Gao, S. Wang, A. Lim, L.B. Hai, S. Ramakrishna, Electrospun poly (L-lactide-co-glycolide) biodegradable polymer nanofibre tubes for peripheral nerve regeneration, Nanotechnology 15 (2004) 1459, https://doi.org/10.1088/0957-4484/15/11/014.
[28] M.V. Jose, V. Thomas, Y. Xu, S. Bellis, E. Nyairo, D. Dean, Aligned bioactive multi-component nanofibrous nanocomposite scaffolds for bone tissue engineering, Macromol. Biosci. 10 (2010) 433–444, https://doi.org/10.1002/mabi.200900287.
[29] C.J. Druesedow, C. Batur, M. Cakmak, B. Yalcin, Pressure control system for electrospinning process, Polym. Eng. Sci. 50 (2010) 800–810, https://doi.org/10.1002/pen.21587.
[30] S. De Vrieze, T. Van Camp, A. Nelvig, B. Hagström, P. Westbroek, K. De Clerck, The effect of temperature and humidity on electrospinning, J. Mater. Sci. 44 (2009) 1357, https://doi.org/10.1007/s10853-008-3010-6.
[31] D.N. Rockwood, R.C. Preda, T. Yucel, X. Wang, M.L. Lovett, D.L. Kaplan, Materials fabrication from Bombyx mori silk fibroin, Nat. Protoc. 6 (2011) 1612–1631, https://doi.org/10.1038/nprot.2011.379.
[32] F. Sadeghian-Nodoushan, R. Aflatoonian, Z. Borzouie, F. Akyash, F. Fesahat, M. Soleimani, S. Aghajanpour, H.D. Moore, B. Aflatoonian, Pluripotency and differentiation of cells from human testicular sperm extraction: An investigation of cell stemness, Mol. Reprod. Dev. 83 (2016) 312–323, https://doi.org/10.1002/mrd.22620.
[33] A. Alessandrino, B. Marelli, C. Arosio, S. Fare, M. Tanzi, G. Freddi, Electrospun silk fibroin mats for tissue engineering, Eng. Life Sci. 8 (2008) 219–225, https://doi.org/10.1002/elsc.200700067.
[34] J. Huang, L. Liu, J. Yao, Electrospinning of Bombyx mori silk fibroin nanofiber mats reinforced by cellulose nanowhiskers, Fibers Polym. 12 (2011) 1002–1006, https://doi.org/10.1007/s12221-011-1002-7.
[35] H.Y. Mi, X. Jing, M.R. Salick, T.M. Cordie, X.F. Peng, L.S. Turng, Properties and fibroblast cellular response of soft and hard thermoplastic polyurethane electrospun nanofibrous scaffolds, J. Biomed. Mater. Res. B Appl. Biomater. 103 (2015) 960–970, https://doi.org/10.1002/jbm.b.33271.
[36] M. Rogulska, Polycarbonate-based thermoplastic polyurethane elastomers modified by DMPA, Polym. Bull. (2018) 1–15, https://doi.org/10.1007/s00289-018-2632-3.
[37] B. Ding, C. Li, Y. Miyauchi, O. Kuwaki, S. Shiratori, Formation of novel 2D polymer nanowebs via electrospinning, Nanotechnology 17 (2006) 3685, https://doi.org/10.1088/0957-4484/17/15/011.
[38] L. Bai, Q. Li, X. Duo, X. Hao, W.C.S. Zhang, Y. Feng, Electrospun PCL-PIBMD/SF blend scaffolds with plasmid complexes for endothelial cell proliferation, RSC Adv. 7 (2017) 39452–39464 10/1039/C7RA06253B.
[39] W. Liu, J. Lipner, C.H. Moran, L. Feng, X. Li, S. Thomopoulos, Y. Xia, Generation of electrospun nanofibers with controllable degrees of crimping through a simple, plasticizer-based treatment, Adv Mater. 27 (2015) 2583–2588, https://doi.org/10.1002/adma.201500329.
[40] J. Amirian, S.Y. Lee, B.T. Lee, Designing of combined nano and microfiber network by immobilization of oxidized cellulose nanofiber on polycaprolactone fibrous scaffold, J. Biomed. Nanotechnol. 12 (2016) 1864–1875, https://doi.org/10.1166/jbn.2016.2308.
[41] Z. Abbasi, Nezhad E. Rezaee, V. Moradi, F. Moradi, O. Ahmadi, A. Homafar, Enzymatic degradation of Poly (ε-Caprolactone) and Starch blends bontaining SiO2 nanoparticle by Amyloglucosidase and α-Amylase, Int. J. Nano Dimension 5 (2014) 549–555, https://doi.org/10.1016/j.compscitech.2011.08.017.
[42] A.C.B. Allen, E. Barone, C.O.K. Crosby, L.J. Suggs, J. Zoldan, Electrospun poly(N-isopropyl acrylamide)/poly(caprolactone) fibers for the generation of anisotropic cell sheets, Biomater. Sci. 5 (2017) 1661–1669, https://doi.org/10.1039/c7bm00324b.
[43] H. Cui, P.J. Sinko, The role of crystallinity on differential attachment/proliferation of osteoblasts and fibroblasts on poly (caprolactone-co-glycolide) polymeric surfaces, Front. Mater. Sci. 6 (2012) 47–59, https://doi.org/10.1007/s11706-012-0154-8.
[44] B. Kong, S. Mi, Electrospun scaffolds for corneal tissue engineering: a review, Materials (Basel) 9 (2016) 614, https://doi.org/10.3390/ma9080614.
[45] E.J. Chen, J. Novakofski, W.K. Jenkins, W.D. O'Brien, Young's modulus measurements of soft tissues with application to elasticity imaging, IEEE Trans. Ultrason. Ferroelectr. Freq. Control 43 (1996) 191–194, https://doi.org/10.1109/58.484478.
[46] A.R. Kemper, A.C. Santago, J.D. Stitzel, J.L. Sparks, S.M. Duma, Biomechanical response of human liver in tensile loading, Ann. Adv. Automot. Med. 54 (2010) 15–26.
[47] L.H. Jansen, P.B. Rottier, Some mechanical properties of human abdominal skin measured on excised strips, Dermatology 117 (1958) 65–83, https://doi.org/10.1159/000255569.
[48] M.G. Dunn, F.H. Silver, Viscoelastic behavior of human connective tissues: relative contribution of viscous and elastic components, Connect Tissue Res. 12 (1983) 59–70, https://doi.org/10.3109/03008208309005612.
[49] J.F.M. Manschot, The mechanical properties of human skin in vivo, 1985, [Sl: sn].
[50] S.J. Manoogian, J.A. Bisplinghoff, A.R. Kemper, S.M. Duma, Dynamic material properties of the pregnant human uterus, J. Biomech. 45 (2012) 1724–1727.
[51] C. Rubod, M. Boukerrou, M. Brieu, C. Jean-Charles, P. Dubois, M. Cosson, Biomechanical properties of vaginal tissue: preliminary results, Int. Urogynecol. J. Pelvic Floor Dysfunct. 19 (2008) 811–816, https://doi.org/10.1007/s00192-007-0533-3.
[52] P.A. Martins, A.L. Silva Filho, A.M.R.M. Fonseca, A. Santos, L. Santos, T. Mascarenhas, A.J. Ferreira, Uniaxial mechanical behavior of the human female bladder, Int. Urogynecol. J. 22 (2011) 991–995, https://doi.org/10.1007/s00192-011-1409-0.
[53] M. Centola, A. Rainer, C. Spadaccio, S. De Porcellinis, J.A. Genovese, M. Trombetta, Combining electrospinning and fused deposition modeling for the fabrication of a hybrid vascular graft, Biofabrication. 2 (2010) 014102, , https://doi.org/10.1088/1758-5082/2/1/014102.
[54] N. L'Heureux, N. Dusserre, G. Konig, B. Victor, P. Keire, T.N. Wight, N.A. Chronos, A.E. Kyles, C.R. Gregory, G. Hoyt, R.C. Robbins, T.N. McAllister, Human tissue-engineered blood vessels for adult arterial revascularization, Nat Med. 12 (2006) 361–365, https://doi.org/10.1038/nm1364.
[55] A. Kurane, D.T. Simionescu, N.R. Vyavahare, In vivo cellular repopulation of tubular elastin scaffolds mediated by basic fibroblast growth factor, Biomaterials 28 (2007) 2830–2838, https://doi.org/10.1016/j.biomaterials.2007.02.031.
[56] J.Y. Yu, Y.B. Zhu, Y.Y. Li, W. Dong, F. Xuan, J.H. Mao, C.F. Gong, Fabrication and mechanical properties of decellularized esophageal submucosal matrix, Chin. J. Biomed. Eng. 30 (2011) 312–320.
[57] F. Safshekan, M. Tafazzoli-Shadpour, M. Abdouss, Shadmehr M. Behgam, F. Ghorbani, Investigation of the Mechanical Properties of the Human Tracheal Cartilage, Tanaffos. 16 (2017) 107–114.
[58] M.S. Ju, C.C.K. Lin, C.T. Chang, Researches on biomechanical properties and models of peripheral nerves-a review, J. Biomech. Sci. Eng. 12 (2017) 16–00678, https://doi.org/10.1299/jbse.16-00678.
[59] A. Tamadon, K.H. Park, Y.Y. Kim, B.C. Kang, S.Y. Ku, Efficient biomaterials for tissue engineering of female reproductive organs, Tissue Eng. Regen. Med. 13 (2016) 447–454, https://doi.org/10.1007/s13770-016-9107-0.
[60] J. Lv, L. Chen, Y. Zhu, L. Hou, Y. Liu, Promoting epithelium regeneration for esophageal tissue engineering through basement membrane reconstitution, ACS Appl. Mater. Interfaces 6 (2014) 4954–4964, https://doi.org/10.1021/am4059809.